Defibrillation Failure and Tachycardia-Induced Early Afterdepolarizations: A Simulation Study

Richard Samade, James N. Weiss, Kalyanam Shivkumar, and Boris Y. Kogan

***Abstract*—The prevention of sudden cardiac death (SCD), frequently caused by ventricular fibrillation (VF), is commonly accomplished with defibrillation shocks. Nevertheless, incidences of defibrillation failure have been reported in practical applications and physiological investigations, the mechanisms of which have not been fully explained. Physiological experiments have suggested that intracellular Ca (Ca_i) dynamics may play a role in reinitiating VF via triggered activity, resulting in defibrillation failure. We hypothesize that defibrillation failure can occur due to spontaneous Ca release from the sarcoplasmic reticulum (SR) and subsequent early afterdepolarizations (EADs), which are caused by Ca_i accumulation in fibrillating tissue. This hypothesis was tested with computer simulations of two-dimensional (2D) tissue that incorporated: a bidomain representation of tissue; an action potential model that exhibits Ca_i dynamics with parameter changes facilitating the appearance of EADs; a fixed distribution of the applied shock current; and a mathematical model of the electroporation phenomenon. We found that when EAD clusters appeared due to rapidly rotating spiral waves in 2D tissue, they facilitated defibrillation failure via triggered activity that produced additional spiral waves after shock application. Similar triggered activity phenomena may be observed with delayed afterdepolarizations and represent a topic for an additional investigation.**

***Index Terms*—computer simulation, defibrillation failure, early afterdepolarizations, mathematical modeling.**

I. Introduction

Electrical defibrillation of the heart is widely regarded by clinicians to be the most effective method for terminating ventricular fibrillation (VF), the major cause of sudden cardiac death (SCD). Despite these achievements, cases of defibrillation failure have been observed in medical practice [1] and physiological experiments [2].

A physiological study by Zaugg *et al* demonstrated that elevated levels of intracellular calcium (Ca_i) mediated the reinitiation of VF during shock failure, implicating a role for Ca dynamics in defibrillation efficacy [3]. Despite these results, a detailed understanding of the mechanisms underlying VF reinitiation after defibrillation does not currently exist. In addition, the majority of previous computer simulation studies [4]-[6] did not utilize a model with Ca_i dynamics. Investigations that did use such a model [7]-[8] did not examine the role of Ca_i dynamics in defibrillation failure.

Our previous investigations, in the absence of defibrillation, showed that early afterdepolarizations (EADs) induced by tachycardia could reinitiate spiral waves in simulated two- (2D) [9]-[11] and three-dimensional (3D) [21] tissues that would have otherwise self-terminated. These simulations utilized a mathematical model of the ventricular action potential (AP) that typically exhibits spontaneous Ca release from the sarcoplasmic reticulum (SR) in the presence of Ca overload in the SR and myoplasm (J_{spon}) [12]. We hypothesized that defibrillation failure can occur due to J_{spon} and subsequent EADs, which are caused by Ca_i accumulation in fibrillating tissue. These EADs form synchronized cellular clusters in tissue and reinitiate spiral waves after the end of shock application. To verify this hypothesis, we used computer simulations with a mathematical model of 2D tissue consisting of: a bidomain representation of tissue [13], an AP model [12] with developed Ca_i dynamics that includes J_{spon} and cell parameter modifications that facilitate the appearance of EADs, a fixed distribution of the applied shock current, and the inclusion of an additional mathematical model that reproduces the phenomenon of electroporation [16]. In the following presentation, the results were obtained under conditions of uniform fiber orientation.

These results validated our hypothesis that tachycardia-induced EADs under conditions of Ca_i accumulation may produce defibrillation failure.

II. Methods

Mathematical models for computer simulation of defibrillation include a bidomain (composed of intracellular and extracellular regions) representation of cardiac tissue [13] and consider the myocardium as a syncitium [14]. The study of excitation-propagation processes in tissue, in the presence of a defibrillation shock, give rise to the following system of equations

$$\nabla \cdot \left(\hat{\sigma}_i \nabla \Phi_i \right) = \beta_{sv} I_m \quad (1)$$

$$\nabla \cdot \left(\hat{\sigma}_e \nabla \Phi_e \right) = -\beta_{sv} I_m - I_{shock} \quad (2)$$

$$V_m = \Phi_i - \Phi_e \quad (3)$$

Manuscript received July 21, 2008. This work was supported in part by the National Heart, Lung, and Blood Institute under both Program Project Grant P01 HL-078931 and Research Project Grant R01 HL-084261. Support was also provided by the Laubisch and Kawata Endowments. Supercomputing resources were provided by the National Energy Research Scientific Computing Center, Office of Energy Research of the United States Department of Energy, under contract no. DEAC0376SF00098.

R. Samade is a Ph.D. student with the Department of Bioengineering, University of California, Los Angeles, Los Angeles, CA 90095 USA (email: rsamade@ucla.edu).

J. N. Weiss is with the Department of Medicine (Cardiology), David Geffen School of Medicine, University of California, Los Angeles, Los Angeles, CA 90095 (email: jweiss@mednet.ucla.edu).

K. Shivkumar is with the Department of Medicine (Cardiology), David Geffen School of Medicine, University of California, Los Angeles, Los Angeles, CA 90095 (email: kshivkumar@mednet.ucla.edu).

B. Y. Kogan is with the Department of Computer Science, University of California, Los Angeles, Los Angeles, CA 90095 USA (phone: 310-825-7393; fax: 310-825-2273; email: kogan@cs.ucla.edu).

$$I_m = \beta_{sv}\left(C_m \frac{\partial V_m}{\partial t} + I_{ion} + I_{stim}\right). \quad (4)$$

If we perform a substitution of (3) and (4) into (1) and then substitute the resulting equation for I_m into (2), we obtain

$$\frac{\partial V_m}{\partial t} = \frac{1}{\beta_{sv} C_m}\left(\nabla\cdot\left(\hat{\sigma}_i \nabla V_m\right) + \nabla\cdot\left(\hat{\sigma}_i \nabla \Phi_e\right)\right) - \frac{1}{C_m}\left(I_{ion} + I_{stim}\right) \quad (5)$$

$$\nabla\cdot\left(\left(\hat{\sigma}_i + \hat{\sigma}_e\right)\nabla\Phi_e\right) = -\nabla\cdot\left(\hat{\sigma}_i \nabla V_m\right) - I_{shock}, \quad (6)$$

with homogeneous Neumann boundary conditions and appropriate initial conditions. In (5) and (6), $\hat{\sigma}_i$ and $\hat{\sigma}_e$ are the conductivity tensors for the intracellular and extracelluar domains, respectively (mS/cm). They reflect variable fiber orientation that is present in 3D tissue. Other variables in (1)-(6) are: I_m, the transmembrane current (μA/cm^2); I_{shock}, a shock current that is applied only to the extracellular domain (μA/cm^3); β_{sv}, the myocyte surface-to-volume ratio (cm^{-1}); C_m, the membrane capacitance per unit area (μF/cm^2); I_{ion}, the sum of transmembrane currents (μA/cm^2); I_{stim}, a transmembrane stimulus current (μA/cm^2); Φ_i, the intracellular potential (mV); Φ_e (mV); V_m, the transmembrane potential (mV); and t, time (ms).

For our purposes, assuming no variable fiber orientation but recognizing the presence of anisotropy in both domains between the longitudinal and transverse directions, (5)-(6) for 2D tissue reduce to the following equations

$$\frac{\partial V_m}{\partial t} = D_{i,x}\frac{\partial^2 V_m}{\partial x^2} + D_{i,y}\frac{\partial^2 V_m}{\partial y^2} + D_{i,x}\frac{\partial^2 \Phi_e}{\partial x^2} + D_{i,y}\frac{\partial^2 \Phi_e}{\partial y^2} - \frac{\left(I_{ion} + I_{stim}\right)}{C_m} \quad (7)$$

$$\frac{\partial^2 \Phi_e}{\partial x^2} + \alpha\frac{\partial^2 \Phi_e}{\partial x^2} = -\frac{g_{i,x}}{\gamma_g}\frac{\partial^2 V_m}{\partial x^2} - \frac{g_{i,y}}{\gamma_g}\frac{\partial^2 V_m}{\partial y^2} - \frac{I_{shock}}{\gamma_g}. \quad (8)$$

In (7)-(8), $D_{i,x} = g_{i,x}/\left(\beta_{sv} C_m\right)$ and $D_{i,y} = g_{i,y}/\left(\beta_{sv} C_m\right)$ are the diffusivities along the x- and y-axes, respectively (cm^2/ms), $\gamma_g = g_{i,x} + g_{e,x}$, $\alpha = \left(g_{i,y} + g_{e,y}\right)/\left(g_{i,x} + g_{e,x}\right)$, $g_{i,x}$, $g_{e,x}$, $g_{i,y}$, and $g_{e,y}$ are conductances where the subscripts i, e, x, and y refer to intracellular, extracellular, x-direction, and y-direction, respectively (mS/cm). Since the size of the 2D tissue (3.2 cm by 3.2 cm) is relatively small, it exhibits uniform fiber orientation. Therefore, we needed to select a shock current distribution that provides a nonlinear distribution of Φ_e $\left(\nabla\cdot\left(\left(\hat{\sigma}_i + \hat{\sigma}_e\right)\nabla\Phi_e\right) = \left(\hat{\sigma}_i + \hat{\sigma}_e\right)\nabla^2\Phi_e = -\nabla\cdot\left(\hat{\sigma}_i \nabla V_m\right) - I_{shock}\right)$. For the sake of simplicity, we chose a linear one-dimensional distribution of the shock current, given as $I_{shock} = f(x) = -ax - b$. For any particular value of x, the value of Φ_e remains constant along the y-direction. Our experience has shown that Φ_e induced by the shock current is several orders of magnitude larger in comparison to that induced by V_m due to wave propagation in tissue. Therefore, it is possible to make an approximation in (8) where the V_m-dependent terms that reflect the ionic currents are neglected. Equation (8) can now be expressed as the following system of equations

$$\frac{\partial^2 \Phi_e}{\partial x^2} = -\frac{I_{shock}}{\gamma_g} = -\frac{ax + b}{\gamma_g} \quad (9)$$

$$\frac{\partial^2 \Phi_e}{\partial y^2} = 0, \quad (10)$$

where a = -2b/L (μA/cm^4) and b (μA/cm^3) are constants that determine the gradient of Φ_e only during shock application and L = 3.2 cm is the size of the tissue along the x-direction. The solution of (9) for the case when a = -1.07x10^6 μA/cm^4 and b = 1.71x10^6 μA/cm^3 is presented in Figure 1 and shows the nonlinear character of the resulting distribution of Φ_e in a spatial scale corresponding to the size of the tissue. Therefore, the complete system of equations for the chosen type of shock current can be reduced into one equation by substituting (9) and (10) into (7)

$$\frac{\partial V_m}{\partial t} = D_{i,x}\frac{\partial^2 V_m}{\partial x^2} + D_{i,y}\frac{\partial^2 V_m}{\partial y^2} - D_{i,x}\frac{ax + b}{\gamma_g} - \frac{\left(I_{ion} + I_{stim}\right)}{C_m}. \quad (11)$$

Equation (11) constitutes the only equation solved during the shock application.

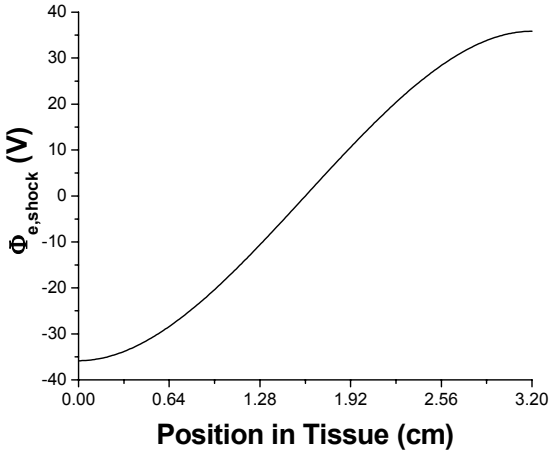

FIGURE 1: **Extracellular potential during shock current application. The spatial distribution of Φ_e produced by a shock current with parameters a = -1.07x10^6 μA/cm^4 and b = 1.71x10^6 μA/cm^3 is shown for the tissue size used in the study.**

A system of nonlinear ordinary differential equations that describes all membrane current components of I_{ion} and relevant intracellular compartment processes is needed to make (7) a closed form expression. For this purpose, we selected the model of guinea pig ventricular AP proposed by Luo and Rudy [15] and with subsequent Ca dynamics modifications by Chudin [12]. All initial conditions and parameters not explicitly shown in (7)-(8) were taken from [12]; parameters described in the preceding paragraph were taken from [6], with the exception that $g_{e,x}$ = 38.8 mS/cm

and $g_{e,y}$ = 2.56 mS/cm. Fibrillation in the 257 by 257 node 2D tissue was performed with the commonly-used S1-S2 pacing protocol (for details, see [10]). In order to amplify the effect of J_{spon} on V_m and produce EADs, we changed three cell parameters (corresponding to long QT 2 syndrome, abbreviated as LQT2), as done in [9].

Defibrillation of the spiral wave was performed after sufficient time was allowed for Ca_i accumulation to occur in tissue. In order to account for the phenomenon of electroporation due to large values of V_m induced by shocks, we incorporated an electroporation current, as was done previously [16].

The computation complexity of our complete bidomain model of defibrillation required the use of massively parallel supercomputers. For this purpose, we used an operator splitting algorithm [17] (see details in [18] for our considered problem). Equation (8) is solved with the full multigrid algorithm [19] using the result of (7) during each Δt (except during the shock, when only (11) is solved. State variable values prior to the start of the shock serve as initial conditions for the next 10 ms. The time and space step of the simulation were Δt = 0.1 ms and h = 0.0125 cm, respectively, and were chosen so that appropriate stability conditions for the numerical solution were satisfied, as described in [10]. Model code was written in the C++ programming language and all computer simulations were performed on massively parallel IBM p575 clusters. Interprocessor communications utilized Message Passing Interface (MPI) in order to distribute the regions of the tissue among processors.

III. Results

A. Determination of Shock Efficacy

In order to determine the shock strength sufficient to terminate reentry, several simulations were conducted using baseline (non-EAD generating) parameters and a sample of these experiments is summarized in Figure 2. After induction of a reentrant wave using S1-S2 protocol, approximately 1 second passes before the wave becomes established (Figure 2*AB*, t = 0.95 s). As Ca_i begins to accumulate due to the high frequency stimulation of the tissue's nodes (f = 6.25 Hz), wavelength increases to the point that wavefront distortion occurs (Figure 2*AB*, t = 2.64 s). Application of a relatively weak shock (a = -7.14x10^5 μA/cm^4 and b = 1.14x10^6 μA/cm^3) led to the termination of the initial reentrant activity (Figure 2*A*, t = 2.65 s to 2.80 s). However, a small region of tissue in the upper left corner remained depolarized long enough to excite neighboring tissue exiting their refractory phase (Figure 2*A*, t = 2.80 s). This led to regeneration of the reentrant wave (Figure 2*A*, t = 2.93 s).

In contrast, a stronger magnitude shock (a = -1.07x10^6 μA/cm^4 and b = 1.71x10^6 μA/cm^3) prolonged refractoriness of the tissue to the point that no spiral wave regeneration could occur (Figure 2*B*, t = 2.80 s). As a consequence, the tissue returned to rest 275 ms after the shock application (Figure 2*B*, t = 2.93 s). This would be within the pacing duration of tissue by a normal sinus rhythm.

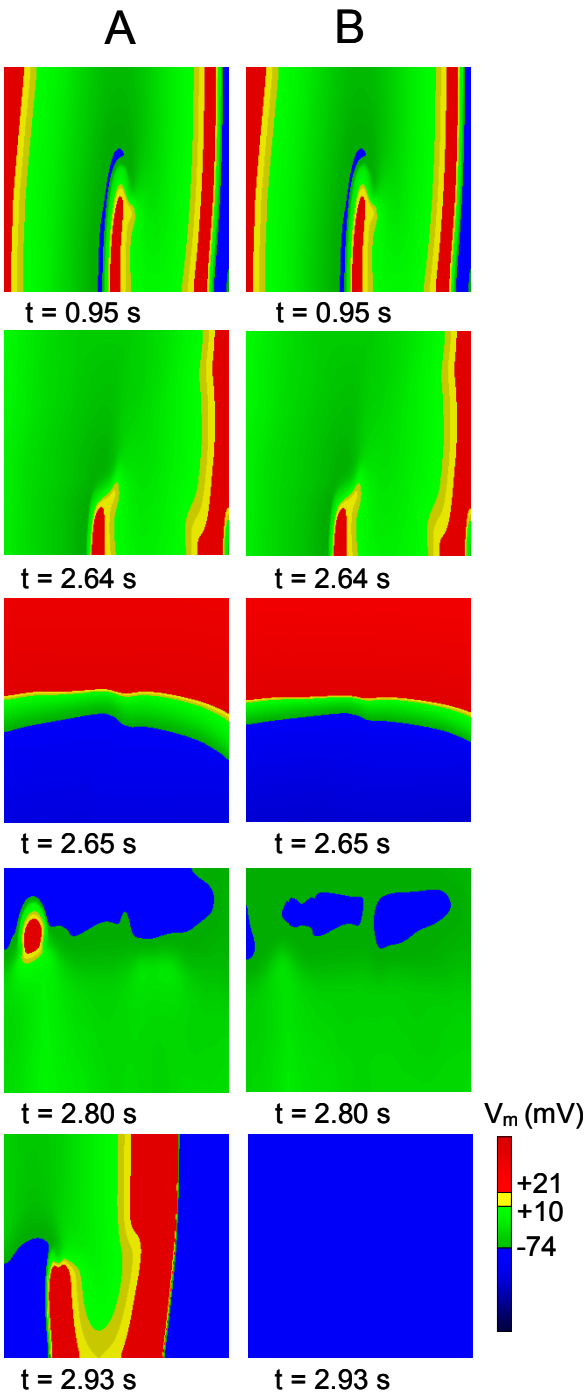

FIGURE 2: **Determination of effective defibrillation shocks in tissue. (*A*) Maps of V_m for a simulated reentrant wave in cardiac tissue are shown at various moments in time prior to and after applying a shock current with parameters a = -7.14x10^5 μA/cm^4 and b = 1.14x10^6 μA/cm^3. (*B*) Maps of V_m under the same conditions as in (*A*), but using a shock current with parameters a = -1.07x10^6 μA/cm^4 and b = 1.71x10^6 μA/cm^3. In both cases, the shock is applied in the time interval between 2.645 and 2.655 s, with the anodal end located on the top and the cathodal end on the bottom.**

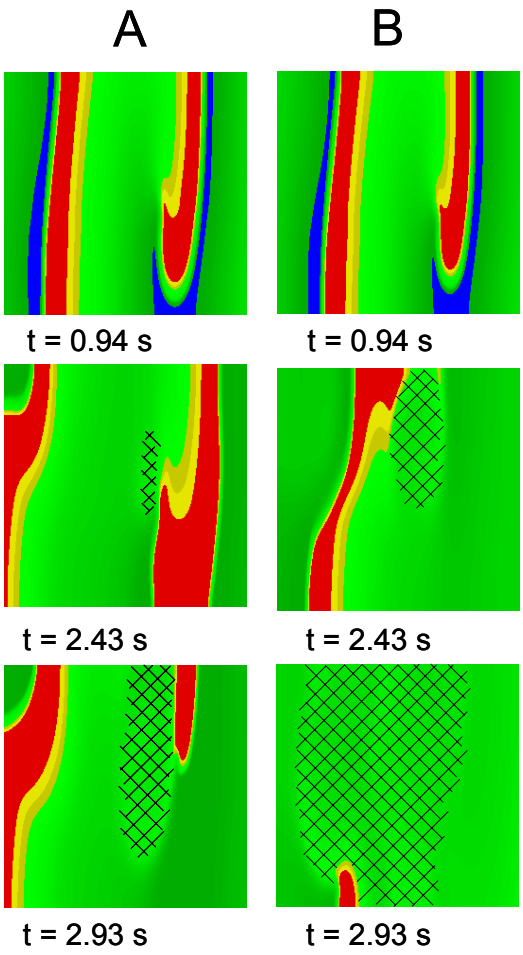

FIGURE 3: **Effect of EADs in producing repolarization failure in tissue. (*A*) Maps of V_m are shown at various moments in time when I_{Kr} is decreased by 10% from baseline. (*B*) Maps of V_m at various moments in time when I_{Kr} is decreased by 20% from baseline. Cross-hatched regions denote EAD clusters.**

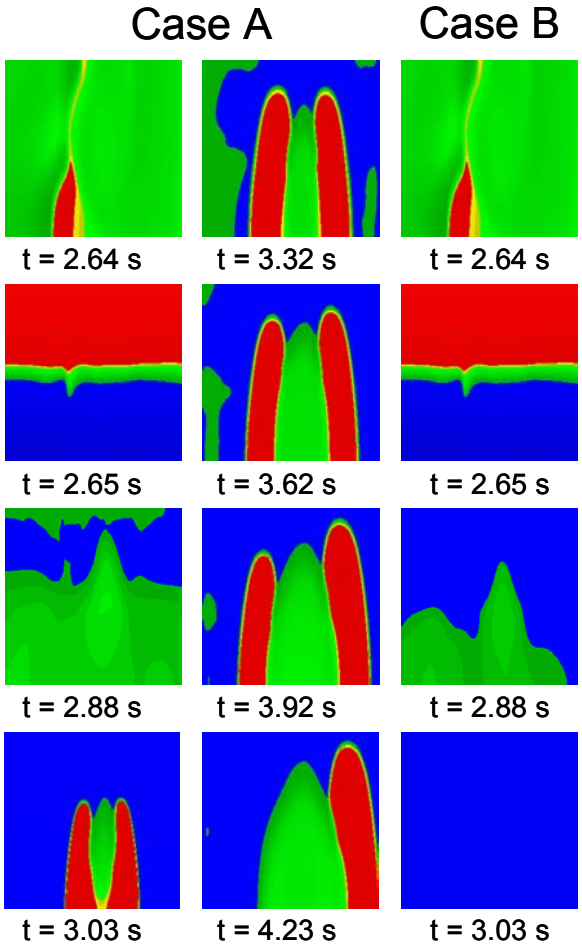

FIGURE 4: **Effect of J_{spon} on sustaining EADs and triggered activity after defibrillation. (Case *A*) Maps of V_m are shown at various moments in time when J_{spon} is not disabled. (Case *B*) Maps of V_m under the same experimental conditions as in (Case *A*), but with J_{spon} disabled at t = 2.77 s.**

In summary, these results show that simulated reentry in our 2D tissue model can be immediately extinguished if the applied shock has parameter values a = -1.07x10^6 μA/cm^4 and b = 1.71x10^6 μA/cm^3.

B. Facilitation of EAD Appearance in Tissue

Introduction of LQT2 parameter changes to our AP model (achieved by a reduction of I_{Kr}, the rapid component of the delayed rectifier potassium current) in order to facilitate the appearance of EADs led to prolongation of the AP duration (APD) and earlier distortions in the wavefront compared to the normal case (Figure 3*AB*, t = 0.94 s). In the case of a 10% reduction of I_{Kr} relative to baseline (Case A), an additional 1.5 s of simulation time needed to pass before a synchronized cluster of EADs was apparent (Figure 3*A*, t = 2.43 s). At the same point in time, tissue with a 20% reduction of I_{Kr} compared to baseline (Case B) exhibits a larger region of EADs than Case A (Figure 3*B*, t = 2.43 s). In addition, the region of EADs in Case B appeared 200 ms earlier than in Case A.

After the onset of EADs in Case A, the cluster increases in size for the next 0.5 s until the original reentrant wave is displaced off the tissue and a new wave arises from the opposite side of the EAD cluster (Figure 3*A*, t = 2.93 s). During the same time period, the region of EADs in Case B grows over time to encompass more than half the tissue (Figure 3*B*, t = 2.93 s).

In conclusion, the size of the EAD clusters increases as the repolarization reserve decreases (accomplished in our particular case by the reduction of I_{Kr}).

C. J_{spon} is Needed for Postshock Reinitiation Due to EADs

The final portion of our investigation centered on what role Ca_i dynamics played in sustaining EAD clusters. For this purpose, a control experiment was devised with I_{Kr} decreased by 20% from baseline and with the shock current as used in Figure 2*B* (a = -1.07x10^6 μA/cm^4 and b = 1.71x10^6 μA/cm^3). The experimental case had identical parameter changes, but at t = 2.77 s, J_{spon} was disabled by setting it equal to zero in the model. In addition, the same magnitude and duration of

the shock as used in Figure 2*B* was utilized and applied at the same time.

After application of the shock, the control case exhibits a remnant of the original EAD cluster (Figure 4, Case *A*, t = 2.88 s), which then migrates to the bottom center of the tissue (Figure 4, Case *A*, t = 2.88 s to t = 3.03 s). From that point in time forward, it reinitiates four different instances of two waves rotating in opposite directions. In each reinitiation event, the two reentrant waves merge into one and propagate toward the top of the tissue (Figure 4, Case *A*, t = 3.03 s, t = 3.32 s, t = 3.62 s, t = 3.92 s). After the fourth pair of waves propagates off the tissue, a sole spiral wave is then reinitiated that rotates in the counterclockwise direction toward the bottom left corner of the tissue (Figure 4, Case *A*, t = 4.23 s).

In contrast to the control case, the experimental case exhibits disappearance of the EAD cluster, commencing immediately after J_{spon} was disabled (Figure 4, Case *B*, t = 2.88 s). Within 380 ms after application of the defibrillation shock, the tissue returns to rest (Figure 4, Case *B*, t = 3.03 s). This corresponds to the time that the first reinitiation event was observed when J_{spon} was not inactivated (Figure 4, Case *A*, t = 3.03 s).

A comparison of the findings from Cases *A* and *B* shows that J_{spon}, is necessary for EAD clusters to persist and produce spiral wave reinitiation after what would otherwise have been a successful defibrillation shock. Thus, J_{spon} produces the necessary reduction in repolarization reserve so that EAD clusters in tissue may occur and reinitiate fibrillation.

IV. Discussion

Physiological experiments have shown that post-shock reinitiation of VF after defibrillation becomes more probable as VF duration lengthens and Ca_i overload becomes more pronounced [3]. In our previous investigations [9]-[11], it was demonstrated that Ca_i accumulation due to spiral waves in tissue played a role in EAD cluster genesis via J_{spon} activation. Thus, we propose that tachycardia-induced EADs in the presence of Ca_i overload could be one of the possible mechanisms for defibrillation failure (for alternative mechanisms, see [2], [5], and [7]). Validation of this hypothesis using physiological experiments has met significant difficulties till now. Computer simulation as an alternative approach requires the use of a bidomain model of tissue during defibrillation with developed Ca_i dynamics. In addition, large shock currents are applied to the membrane, necessitating the reproduction of the membrane electroporation phenomenon. In the general case of 3D tissue, one must consider variable fiber orientation, as shown in (5) and (6). For our case, where a relatively small section of 2D tissue was utilized, it is possible to neglect variable fiber orientation and reduce the general bidomain equations into the particular equations (7) and (8). The effect of the V_m -dependent terms due to wave propagation in (8) can be neglected when compared to the effect of the shock current. Our experience has shown that $|\Phi_e|_{\max} < 50\,\text{mV}$ without the shock and $|\Phi_e|_{\max} \cong 36\,\text{V}$ due to the shock. Choosing the specific linear form of the shock current, we reduce (7) and (8) into one equation (11). These simplifications introduce only a small quantitative difference in the postshock distribution of V_m. As a result, we were able to overcome computational difficulties and prove our hypothesis.

Utilization of the above considerations allowed us to divide the entire time course of our simulations into three parts: prior, during, and after the shock application. The first and third parts require the solution of a reaction-diffusion equation (7) and an elliptic equation (8). However, during the period of shock application, it is only necessary to solve (11).

The limitations of our study are connected with a lack of detailed physiological data concerning J_{spon}. For this reason, our results might be considered to have only qualitative, but not quantitative, relevance to more general cases.

In summary, this study of the role of tachycardia-induced EADs during Ca_i overload demonstrated that when EAD clusters were present in 2D tissue, they facilitated defibrillation failure by reinitiating spiral waves. This was found to be determined by Ca_i overload that affected the appearance of EADs via J_{spon} activation, since disabling J_{spon} led to immediate repolarization of the entire tissue. Similar reinitiation could be observed with DADs and deserve to be the topic of a separate investigation.

References

[1] H. Lui, K. Axtell, M. Biehl, S. Deshpande, A. Dhala, Z. Blanck, J. Sra, M. Jazayeri, and M. Akhtar. (1996, November). Sudden death in patients with implanatable cardioverter defibrillators. *Am. Heart J.* [Online]. *132(5)*. pp. 986-988. Available: http://www.ncbi.nlm.nih.gov/pubmed/8892772

[2] G-S. Hwang, H. Hayashi, L. Tang, M. Ogawa, H. Hernandez, A. Y. Tan, H. Li, H. Karagueuzian, J. N. Weiss, S-F. Lin, and P-S. Chen. (2006, December). Intracellular calcium and vulnerability to fibrillation and defibrillation in Langendorff-perfused rabbit ventricles. *Circulation* [Online]. *114(24)*. pp. 2595-2603. Available: http://circ.ahajournals.org/cgi/content/abstract/114/24/2595

[3] C. E. Zaugg, S. T. Wu, V. Barbosa, P. T. Buser, J. Wikman-Coffelt, W. W. Parmley, and R. J. Lee. (1998, November). Ventricular fibrillation-induced intracellular Ca(2+) overload causes failed electrical defibrillation and post-shock reinitiation of fibrillation. *J. Mol. Cell. Cardiol.* [Online]. *30(11)*. pp. 2183-2192. Available: http://www.ncbi.nlm.nih.gov/pubmed/9925356

[4] J. P. Keener and A. V. Panfilov. (1996, September). A biophysical model for defibrillation of cardiac tissue. *Biophys. J.* [Online]. *71(3)*. pp. 1335-1345. Available: http://www.ncbi.nlm.nih.gov/pubmed/8874007

[5] N. Trayanova, K. Skouibine, and P. Moore. (1998, March). Virtual electrode effects in defibrillation. *Prog. Biophys. Mol. Biol.* [Online]. *69(2-3)*. pp. 387-403. Available: http://www.ncbi.nlm.nih.gov/pubmed/9785947

[6] N. Trayanova, J. Eason, and F. Aguel. (2002, July). Computer simulations of defibrillation: a look inside the heart. *Comput. Vis. Sci.* [Online]. *4(4)*. pp. 259-270. Available: http://www.springerlink.com/content/k9hrlekt47a6ghx2/

[7] T. Maharaj, R. Blake, N. Trayanova, D. Gavaghan, and B. Rodriguez. (2008, January-April). The role of transmural ventricular heterogeneities in cardiac vulnerability to electric shocks. *Prog. Biophys. Mol. Biol.* [Online]. *96(1-3)*. pp. 321-338. Available: http://www.ncbi.nlm.nih.gov/pubmed/17915299

[8] G. Plank, A. Prassl, E. Hofer, and N. A. Trayanova. (2008, March). Evaluating intramural virtual electrodes in the myocardial wedge preparation: simulations of experimental conditions. *Biophys. J.* [Online]. *94(5)*. pp. 1904-1915. Available: http://www.ncbi.nlm.nih.gov/pubmed/17993491

[9] R. Huffaker, S. T. Lamp, J. N. Weiss, and B. Kogan. (2004, October). Intracellular calcium cycling, early afterdepolarizations, and reentry in simulated long QT syndrome. *Heart Rhythm* [Online]. *1(4)*. pp. 441-448. Available: http://www.ncbi.nlm.nih.gov/pubmed/15851197

[10] R. B. Huffaker, J. N. Weiss, and B. Kogan. (2007, June). Effects of early afterdepolarizations on reentry in cardiac tissue: a simulation study. *Am. J. Physiol. Heart Circ. Physiol.* [Online]. *292(6)*. pp. H3089-H3102. Available: http://www.ncbi.nlm.nih.gov/pubmed/17307992

[11] B. Kogan, S. T. Lamp, and J. N. Weiss., "Role of intracellular Ca dynamics in supporting spiral wave propagation," in *Modeling and Simulation*, 1st ed. vol. 1, G. Bekey and B. Kogan, Eds. Boston: Kluwer Academic, 2003, pp. 177–193.

[12] E. Chudin, J. Goldhaber, A. Garfinkel, J. Weiss, and B. Kogan. (1999, December). Intracellular Ca(2+) dynamics and the stability of ventricular tachycardia. *Biophys. J.* [Online]. *77(6)*. pp. 2930-2941. Available: http://www.ncbi.nlm.nih.gov/pubmed/10585917

[13] C. S. Henriquez. (1993). Simulating the electrical behavior of cardiac tissue using the bidomain model. *Crit. Rev. Biomed. Eng.* [Hardcover Book]. *21(1)*. pp. 1-77.

[14] J. C. Neu and W. Krassowska. (1993). Homogenization of syncytial tissues. *Crit. Rev. Biomed. Eng.* [Hardcover Book]. *21(2)*. pp. 137-199.

[15] C. H. Rudy and Y. Rudy. (1994, June). A dynamic model of the cardiac ventricular action potential. I. Simulations of ionic currents and concentration changes. *Circ. Res.* [Online]. *74(6)*. pp. 1071-1096. Available: http://www.ncbi.nlm.nih.gov/pubmed/7514509

[16] K. A. DeBruin and W. Krassowska. (1998, July-August). Electroporation and shock-induced transmembrane potential in a cardiac fiber during defibrillation strength shocks. *Ann. Biomed. Eng.* [Online]. *26(4)*. pp. 584-596. Available: http://www.ncbi.nlm.nih.gov/pubmed/9662151

[17] G. Strang. (1968, September). On the construction and comparison of difference schemes. *SIAM. J. Numer. Anal.* [Online]. *5(3)*. pp. 506-517. Available: http://www.jstor.org/sici?sici=0036-1429(196809)5%3A3%3C506%3AOTCACO%3E2.0.CO%3B2-4

[18] B. Y. Kogan, W. J. Karplus, and E. E. Chudin, "Heart fibrillation and parallel supercomputers," in *Proc. Int. Conf. Inform. Control*, vol. 3, St. Petersburg, Russia, 1997, pp. 225–236.

[19] A. Brandt. (1977, April). Multi-level adaptive solutions to boundary-value problems. *Math. Comput.* [Online]. *31(138)*. pp. 333-390. Available: http://www.jstor.org/sici?sici=0025-5718(197704)31:138%3C333:MASTBP%3E2.0.CO%3B2-M

[20] Y. Cheng, K. A. Mowrey, D. R. Van Wagoner, P. J. Tchou, and I. R. Efimov. (1999, November). Virtual electrode-induced reexcitation: a mechanism of defibrillation. *Circ. Res.* [Online]. *85(11)*. pp. 1056-1066. Available: http://www.ncbi.nlm.nih.gov/pubmed/10571537

[21] R. B. Huffaker, *Tachycardia-Induced Early Afterdepolarizations: Ionic Mechanisms and Effects on Wave Propagation in 1,2, and 3D Tissue (Computer Simulation Study)*. Ph.D. Dissertation, Department of Computer Science, University of California, Los Angeles, Los Angeles, CA, 2008.